OPTICS

# Observation of nonreciprocal magnetophonon effect in nonencapsulated few-layered $CrI_3$

**Zhen Liu[1]*, Kai Guo[1]*, Guangwei Hu[2], Zhongtai Shi[1], Yue Li[1], Linbo Zhang[1], Haiyan Chen[1], Li Zhang[1], Peiheng Zhou[1], Haipeng Lu[1], Miao-Ling Lin[3], Sizhao Liu[4], Yingchun Cheng[4], Xue Lu Liu[3], Jianliang Xie[1], Lei Bi[1], Ping-Heng Tan[3], Longjiang Deng[1†], Cheng-Wei Qiu[2†], Bo Peng[1†]**



**"Magneto-optical" effect refers to a rotation of polarization plane, which has been widely studied in traditional ferromagnetic metal and insulator films and scarcely in two-dimensional layered materials. Here, we uncover a new nonreciprocal magnetophonon Raman scattering effect in ferromagnetic few-layer $CrI_3$. We observed a rotation of the polarization plane of inelastically scattered light between −20° and +60° that are tunable by an out-of-plane magnetic field from −2.5 to 2.5 T. It is experimentally observed that the degree of polarization can be magnetically manipulated between −20 and 85%. This work raises a new magneto-optical phenomenon and could create opportunities of applying two-dimensional ferromagnetic materials in Raman lasing, topological photonics, and magneto-optical modulator for information transport and storage.**

## INTRODUCTION

Ferromagnetic ordering at the monolayer limit was believed to be prohibited at nonzero temperature according to the Mermin-Wagner theorem (*1*); however, recent discoveries of Ising ferromagnetism in monolayer $CrI_3$ and $Cr_2Ge_2Te_6$ prove that there remain exciting possibilities of magnetism at the atomic-scale thickness in two-dimensional (2D) material (*2*, *3*). The rich physics of the magneto-optical effect and spin manipulation in 2D ferromagnetic van der Waals (vdW) material remains to be extensively explored (*4*–*8*). The long-range magnetic orders together with their rich electronic and optic properties in 2D layered materials could open up numerous opportunities for topological photonics, spintronics, and information storage applications (*9*–*16*).

Atomically thin $CrI_3$ is a typical 2D Ising ferromagnetic material with a Curie temperature ($T_C$) of ~45 K (*3*, *17*). The ferromagnetic nature originates from the $Cr^{3+}$ ions with electronic configuration $3d^3$; the magnetic moment is aligned in the out-of-plane direction perpendicular to the $CrI_3$ layer. Beyond the monolayer, the vdW heterostructures comprising layered 2D ferromagnetic materials have been studied as magnetic tunneling junction devices, showing promise for next-generation information transfer and data storage technologies (*12*, *13*, *18*). Moreover, feasible approaches to switch the magnetic orders between ferromagnetic and antiferromagnetic states through electric gating or electrostatic doping (*19*–*21*) and pressure (*22*, *23*) have been demonstrated, again providing more opportunities for the reliable 2D magnetic devices.

However, to date, the magneto-optical effect in layered 2D ferromagnetic materials is rarely explored except for the Kerr effect (*24*). For example, magnetic fields tune inter-Landau–level excitations in resonance with the phonon by electron-phonon coupling, resulting in a pronounced anticrossing behavior of the coupled phonon and electronic modes in nonmagnetic graphene (*25*, *26*). As a simple physical picture, the Lorentz oscillator mode gives the polarizability and permittivity of materials via the kinetic equation of motion; in the presence of an applied out-of-plane magnetic field ($\vec{\mathbf{B}} \| \hat{\mathbf{z}}$) that leads to a Lorentz force $eB\dot{r}$, the kinetic equation is modified as is given $m\ddot{r} + m\gamma\dot{r} + m\omega_0^2 r(\omega) + eB\dot{r} = -eE$. This indicates that the polarizability and permittivity can be controlled by magnetic field (*27*, *28*), thus suggesting marked inelastic phonon scattering behavior controllable with magnetic field. This phenomenon has rarely been reported until now. This missing scenario may hinder the full manipulation of photons, electrons, and spins, especially phonons in atomically thin magnetic materials as well as the exciting applications based on the magneto-optical effect.

Here, we report a phenomenal effect of nonreciprocal magnetophonon Raman scattering. Specifically, the low-temperature polarization angle–resolved confocal Raman system with the external magnetic field is used to study anisotropic inelastic phonon scattering. We observe that the polarization axis of the light scattered from trilayer (3L), 5L, and bulk $CrI_3$ rotates from −15°, −8°, −20° to +40°, +35°, +60°, respectively, when an applied out-of-plane magnetic field changes from −2.5 to +2.5 T. The helicity parameter of circularly polarized phonon scattering light can be magnetically tuned between −20 and 85%, which are also nonlinear and nonreciprocal versus magnetic field. Our measurements reveal that the ferromagnetic 2D layered $CrI_3$ is a unique magneto-optical material system that supports the seemingly controversial coexistence between the extremely large rotation angle and short optical path and, thereafter, holds great promise for nonreciprocal magneto-optical devices, especially in Raman lasing toward photonic integrated circuit and on-chip devices (*29*–*32*).

## RESULTS

The $CrI_3$ bulk crystals were synthesized by the chemical vapor transfer method (*17*). Although the bulk is monoclinic (space group C2/m; see section S1) at room temperature, the few-layer and bulk

[1]National Engineering Research Center of Electromagnetic Radiation Control Materials, School of Electronic Science and Engineering, University of Electronic Science and Technology of China, Chengdu 611731, China. [2]Department of Electrical and Computer Engineering, National University of Singapore, 117583, Singapore. [3]State Key Laboratory of Superlattices and Microstructures, Institute of Semiconductors, Chinese Academy of Sciences, P. O. Box 912, Beijing 100083, China. [4]Key Laboratory of Flexible Electronics & Institute of Advanced Materials, Jiangsu National Synergetic Innovation Center for Advanced Materials, Nanjing Tech University, Nanjing 211816, China.
*These authors contributed equally to this work.
†Corresponding author. Email: bo_peng@uestc.edu.cn (B.P.); chengwei.qiu@nus.edu.sg (C.-W.Q); denglj@uestc.edu.cn (L.D.)

$CrI_3$ is rhombohedral stacking order at 10 K (space group $R\bar{3}$; Fig. 1A), consistent with our previous reports (*33*). The 3L and 5L $CrI_3$ were first exfoliated from the bulk and then directly transferred onto 285-nm $SiO_2$/Si substrates; the nonencapsulated $CrI_3$ were in situ–loaded into a closed cycle optical cryostat in a glovebox. Figure 1B shows the optical micrograph of a 3L $CrI_3$ flake, and the layer number of $CrI_3$ can be identified through the optical contrast (*3*, *33*). The magnetic control of magnetophonon effect is then studied through our low-temperature (10 K) angle-resolved Raman system with an out-of-plane external magnetic field (7 T), which has been excellently calibrated (see Materials and Methods and section S2).

Figure 1C displays the Raman features of 3L, 5L, and bulk $CrI_3$ at 10 K in the absence of magnetic field. The features at ~128 and ~237 $cm^{-1}$ in 3L $CrI_3$ are assigned to the out-of-plane $A_g^3$ mode (*33*, *34*) (the alternate squeezing and spreading of iodine atoms in the out-of-plane direction) and the in-plane $E_g^4$ modes (the alternate displacement of Cr atoms) (*35*, *36*). We observed that the $E_g^4$ features are softened and shift to low frequency as the layer number increases, while the $A_g^3$ features remain unaffected. The frequency difference between the $A_g^3$ and $E_g^4$ modes changes from 109.2, to 108.6, to 107.6 $cm^{-1}$ in 3L, 5L, and bulk $CrI_3$, respectively, indicating the feasibility of identifying the layer number through the frequency difference.

The unambiguous nonreciprocal magnetophonon Raman scattering effect is observed. Figure 1 (D to F) shows the polarization dependence of the $A_g^3$ and $E_g^4$ modes in 3L $CrI_3$ at 10 K excited by a linearly polarized 514-nm light with an incident polarization ($\mathbf{e_i}$) along the *x* axis, defined as 0°. The polarization axis of scattering light ($\mathbf{e_s}$) is rotated in the *x*-*y* plane with θ angle configuration. The Raman intensities of the $E_g^4$ mode almost remain constant in different scattering polarization, indicating that the in-plane $E_g^4$ vibration is isotropic. Furthermore, the isotropic behaviors are independent of the out-of-plane magnetic field (see sections S3 to S5). In stark contrast, the $A_g^3$ mode exhibits a pronounced anisotropic polarization dependence behavior with a twofold rotation symmetric shape. At zero external magnetic fields, the scattering polarization axis of the $A_g^3$ mode is at 5° (see Fig. 1D and section S3). Strikingly, when an external magnetic field is applied, the scattering polarization axis of the anisotropic $A_g^3$ mode is rotated to +40° (−15°) value for +2 T (−2 T). It is interesting to note that the rotation changes its direction and amplitude when the magnetic field with the same magnitude switches the direction (see section S3).

To further verify such exotic magnetophonon effect, we measured the polarization-resolved Raman spectra of 5L and bulk $CrI_3$ under different magnetic fields. Figure 2A shows the polarization dependence of Raman intensities of the $A_g^3$ mode of 5L $CrI_3$ in different magnetic fields. Strikingly, the polarization axis is rotated from −8° to +35° as the magnetic field variates from −2.5 to +2.5 T (see Fig. 2B and section S4). The rotation direction of the polarization axis is opposite when the direction of the magnetic field is reversed; however, the absolute values of polarization rotation angles are not equal in the positive and negative magnetic fields. Such nonreciprocal magnetophonon scattering behaviors are more explicit in bulk $CrI_3$. The polarization axis is slowly rotated to −20° as magnetic field increases from 0 to −2.5 T; however, it is drastically rotated to +60° with increasing magnetic field from 0 to +2.5 T (see Fig. 2B and section S5). In stark contrast, using Si substrates as control samples, the scattering polarizations show no dependence on the magnetic field, although a twofold anisotropic pattern is observed too (see section S6). Therefore, it evidences that the nonreciprocal magnetophonon scattering effect of the anisotropic phonon mode takes place in 2D ferromagnetic $CrI_3$ in the presence of magnetic field.



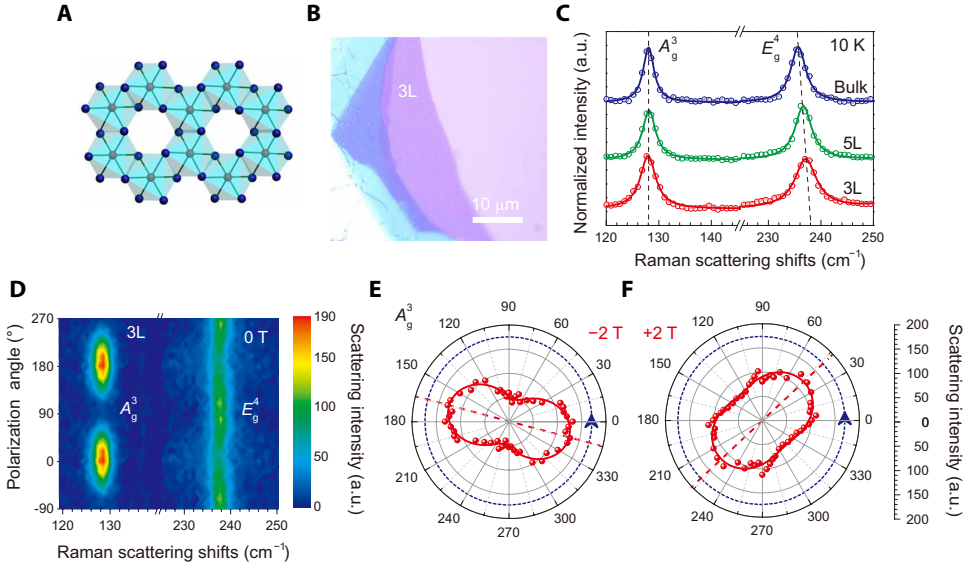


**Fig. 1. Structure of $CrI_3$.** (**A**) Schematic of monolayer $CrI_3$. Red and blue balls represent Cr and I atoms, respectively. The low-temperature crystal structure of $CrI_3$ is rhombohedral (space group $R\bar{3}$), in which $Cr^{3+}$ ions are coordinated by six nonmagnetic $I^-$ ions to form an octahedral geometry, which further share edges to build a honeycomb network. (**B**) The optical images of few-layered $CrI_3$ with an optical contrast of approximately −0.1, which determine the layer number to be 3. (**C**) Raman spectra of 3L, 5L, and bulk $CrI_3$ at 10 K. The $E_g^4$ mode shift to low Raman frequency as the layer number increases. (**D**) 2D maps of phonon scattering spectra of 3L $CrI_3$ at 0 T. (**E** and **F**) Raman scattering intensity of the $A_g^3$ mode of 3L $CrI_3$ as a function of polarization angle under a magnetic field of −2 and +2 T at 10 K. Red dashed line represents the polarization axis of anisotropic scattering, which is rotated from −15° to 40° by the magnetic field. a.u., arbitrary units.

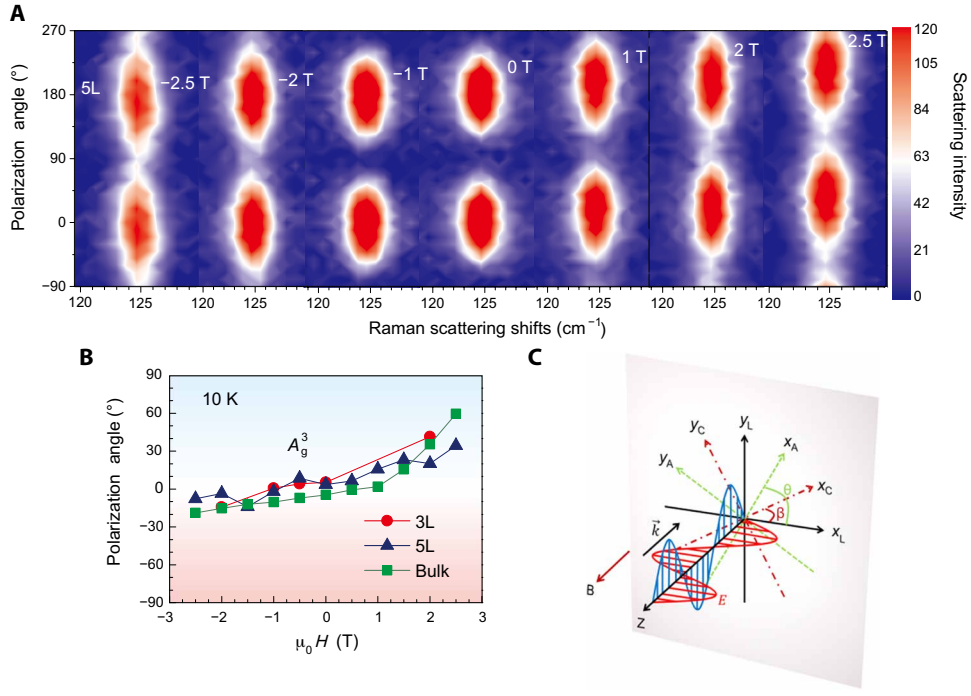


**Fig. 2. Magnetic control of anisotropic scattering.** (**A**) 2D maps of magneto-optical Raman scattering spectra of 5L $CrI_3$ as a function of magnetic field. The polarization plane is rotating as the magnetic field increases. (**B**) Polarization angle of 3L, 5L, and bulk $CrI_3$ with an asymmetric variation as a function of magnetic field, indicating a nonreciprocal magnetic-biased control behavior. (**C**) Schematic picture of polarization configuration. β is the angle between laboratory coordinates ($x_L$, $y_L$, and $z_L$) and crystal coordinates ($x_C$, $y_C$, and $z_C$). θ is the scattering angle in the laboratory coordinates.

The Raman scattering features of the $A_g^3$ and $E_g^4$ modes of 3L, 5L, and bulk $CrI_3$ at different magnetic fields do not offer any detectable difference on the phonon frequency, line width, and shape (see section S7), indicating that the lattice parameters of $CrI_3$ are completely unrelated to the external magnetic field. Thus, the magnetostrictive strain effect, the coupling of phonon and Landau level, and phonon-plasmon coupling are not responsible for the nonreciprocal magnetophonon effect (*25*, *26*, *37*). The unpolarized Raman scattering intensities of the $A_g^3$ and $E_g^4$ modes detected without the polarization analyzer are also independent of magnetic field (see section S8), indicating that magnetic field does not influence the total scattering intensity. Thus, we can safely attribute the magneto-optical Raman scattering effect to magnetic control of the dipole moment of $CrI_3$ lattice vibration (Fig. 3, A and B).

## DISCUSSION

In ferromagnetic materials, the spin-orbital interaction and Heisenberg's exchange interaction lead to a strong effective magnetic field and lift the degeneracy of ground states and excited states together with the external magnetic field, thus resulting in nonreciprocal magneto-optical Faraday and Kerr effect of ferromagnets (*10*, *11*, *38*, *39*). Generally, classic theories have been proposed to explain the magneto-optical Faraday and Kerr effect in ferromagnetic materials: (i) the electron dynamics theory from the Lorentz model and Maxwell's equations and (ii) the macroscopic theory on the basis of the dielectric tensor theory in the constitutive relations solving the Maxwell's equations of electromagnetic wave. The electron dynamics theory from the Lorentz model demonstrates that the polarizability tensor ($\alpha_K$) is strongly dependent on magnetic field (see section S9). From the macroscopic descriptions of scattering, Raman inelastic scattering intensity is intimately connected to the differential scattering cross sections and polarizability tensor, which is given by

$$I = \left[\frac{\langle Q_{K0}\rangle(\omega_0 - \omega_k)^4}{32\pi c^3}\sin^2\varphi\right] |\alpha_K \cdot E|^2 \quad (1)$$

Onsager's relation has proposed that the symmetry of off-diagonal components of the polarizability tensor is broken by a magnetic field because of time inversion symmetry breaking (*40*); thus, $\alpha_{xy} \neq \alpha_{yx}$, and the reciprocity is broken (see sections S9 and S10). The nonreciprocity increases as the ratio of the off-diagonal component to the diagonal component increases. The scattering intensity is maximum only when the dipole moment vector is perpendicular to scattering direction ($\varphi = 90^\circ$); thus, the rotation angle of polarization axis (θ; Fig. 2C) is strongly dependent on $a_{yx}/a_{xx}$. That is to say, the magnetophonon scattering effect originates from the rotation of the dipole moment vector through tuning the polarizability tensor (Fig. 3, A and B).

The few- and monolayer $CrI_3$ have shown Kerr effect and magnetic circular dichroism in the near infrared–visible light region (*3*, *15*, *21*); the ratio of the off-diagonal to diagonal components of the permittivity tensor of few-layer $CrI_3$ is up to ~5%, representing at least one order of magnitude larger than classic ferromagnetic insulator $Ce_1Y_2Fe_5O_{12}$ (CeYIG) and $Bi_1Y_2Fe_5O_{12}$ (BiYIG) (see section S11) (*41*), thus leading to the giant magnetophonon scattering angle up to approximately two orders of magnitude larger than that from the magneto-optical Kerr effect (*24*). Moreover, the $CrI_3$ flakes

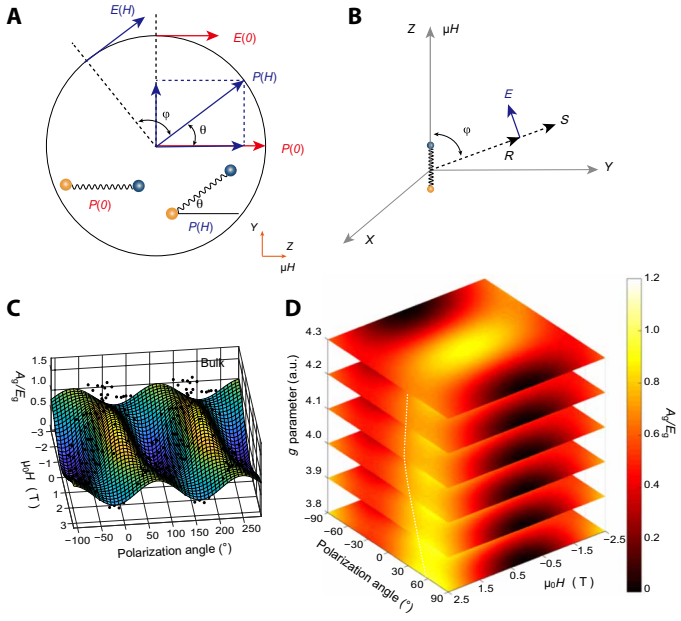


**Fig. 3. Origin of magnetophonon scattering effect.** (**A** and **B**) The vector of induced dipole moment [*P*(0) and *P*(*H*)] is rotated by magnetic field from 0° to θ, leading to the direction of the maximum differential scattering cross sections [*E*(0) and *E*(*H*)] rotating at an angle of θ. φ is the angle between the dipole moment (*P*) and the scattering direction (*R*); *S* represents the Poynting vector; *E* is the electric field vector that is perpendicular to *R* in the plane comprising *R* and *P*. *E*(0) and *E*(*H*) are maximized when φ = 90°. (**C**) All experimental and corresponding calculation (3D color distributions, *g* = 4; fig. S9C) results of the $A_g^3$ mode of bulk $CrI_3$ versus magnetic field and polarization angle, which are well consistent. The intensity ratio of the $A_g^3$ to the $E_g^4$ mode is used to eliminate the system disturbance in the fitting. (**D**) Corresponding calculation results of the $A_g^3$ mode of bulk $CrI_3$ as a function of parameter *g*, magnetic field, and polarization angle.

may be ideal 2D magneto-optical materials and open the door toward nonreciprocal photonic integrated device at optical frequencies (*29*, *30*, *32*). To avoid complex mathematic derivation and focus on the physical essence of magnetophonon scattering effect, the polarizability tensor of the $A_g{}^3$ mode in the presence of magnetic field is simplified to a new Hermitian matrix with magnetic-dependent complex diagonal and off-diagonal components (see sections S9 and S10)

$$\alpha_K^L(A_g(B)) = \frac{e}{\omega}\begin{bmatrix} -\frac{iaB_0}{B_0^2+B^2} & \frac{bB}{B_0^2+B^2} & 0 \\ -\frac{bB}{B_0^2+B^2}c & -\frac{iaB_0}{B_0^2+B^2} & 0 \\ 0 & 0 & \alpha_{zz} \end{bmatrix}$$

The corresponding magneto-optical Raman scattering intensity of $A_g^3$ mode as a function of scattering angle θ is given by

$$I(A_g(B)) \propto \left| -\frac{e}{\omega}\frac{(Bb\sin\theta - ha\cos\theta) + iga\cos\theta}{(g+ih)^2+B^2} \right|^2 \quad (2)$$

where *a* and *b* are the lattice symmetry-restricted elements, and $B_0 = \frac{m(-\omega^2+i\gamma\omega+\omega_0^2)}{ie\omega} = \frac{m\gamma}{e} + i\frac{m(\omega^2-\omega_0^2)}{e\omega} = g + ih$ determines the rotation of polarization axis and ellipticity of the polarized scattering light. All experimental results of the $A_g^3$ modes from 3L, 5L, and bulk $CrI_3$ are together fitted by Eq. 2, in which the experimental and calculated results are in good agreement (Fig. 3C and fig. S9, A to C). The electron moving in an out-of-plane magnetic field experiences an in-plane Lorentz force, which increases the natural frequency ($\omega_0$) in a negative magnetic field. Consequently, the damping constant γ and $B_0$ increase in a negative magnetic field (fig. S9D), while the Lorentz force slows down $\omega_0$ and diminishes $B_0$ in a positive magnetic field (fig. S9E). Therefore, the diagonal and off-diagonal components of the polarizability tensor can be controlled by magnetic field and display different values in negative and positive magnetic fields, enabling the nonreciprocal magnetophonon effect (see section S10 and fig. S10). Figure 3D shows that the rotation angle of the polarization axis increases as the *g* decreases. Strikingly, the nonreciprocal magnetophonon Raman scattering behaviors are predicted by the proposed Lorentz-modified Eq. 2 from the electron dynamics theory. The polarization angle is ~60° in a magnetic field of 2.5 T with *g* = 3.8. On the contrary, the angle changes to approximately −20° when the magnetic field switches to −2.5 T with *g* = 4.3. The experimental results in Fig. 2B are in agreement with the calculation. Thus, the nonreciprocal magnetophonon effect arises from the magnetic field dependence of $B_0$, which tunes both complex diagonal components and off-diagonal components of the polarizability tensor (see sections S9 and S10) (*28*). The magnetic field–dependent behaviors of the inelastic scattering polarization angle mainly arise from the Lorentz force. The magnetic states of $CrI_3$ can influence the nonreciprocal magnetophonon effect. An intrinsic magnetic field of $CrI_3$ flakes below $T_C$ enhances the anisotropic scattering effect, resulting in a nonzero scattering angle at 0 T (*3*, *24*), as shown in Fig. 2B and sections S3 to S5. However, above $T_C$, the nonreciprocity is drastically weakened and almost disappears; the polarization axis of Raman signals is collinear with the laser excitation, giving rise to a zero scattering angle at a zero magnetic field (see section S12) (*24*). The exotic nonreciprocal magnetophonon scattering effect, in which the polarization angle value is asymmetric in the positive and negative magnetic fields (Fig. 2B), deserves future theoretical investigation. It may lead to the better understanding of the fundamental physics of the anomalous nonreciprocal magneto-optical Raman scattering effect in 2D ferromagnetic layered materials. The nonreciprocal magneto-optical scattering effect is observed in ferromagnetic few-layer $CrI_3$, which probably uncovers a new nonreciprocal magneto-optical effect, besides Faraday effect, Kerr effect, and magnetic circular dichroism. Our observation may stimulate both experimental and theoretical investigations of magneto-optical scattering effect (*42*).

The Raman intensity of the $E_g^4$ mode at zero magnetic field is given by $I(E_g) \propto c^2 + d^2$ (see section S13), which confirms its isotropic behaviors. The corresponding magneto-optical Raman scattering intensity of the $E_g^4$ mode in an out-of-plane magnetic field is $I(E_g(B)) \propto \left|\frac{B_0}{B_0^2+B^2}c\right|^2 + \left|\frac{B}{B_0^2+B^2}d\right|^2$ (see section S13). The in-plane $E_g^4$ mode intensities are still independent of the polarization angle, which remains isotropic under magnetic field. Therefore, the $E_g^4$ mode intensity remains almost constant and isotropic in different magnetic fields (see sections S3 to S5).

Furthermore, we demonstrate a magnetic control of degree of polarization (DOP), which allows us to identify and controllably access the parallel and perpendicular polarization configuration.

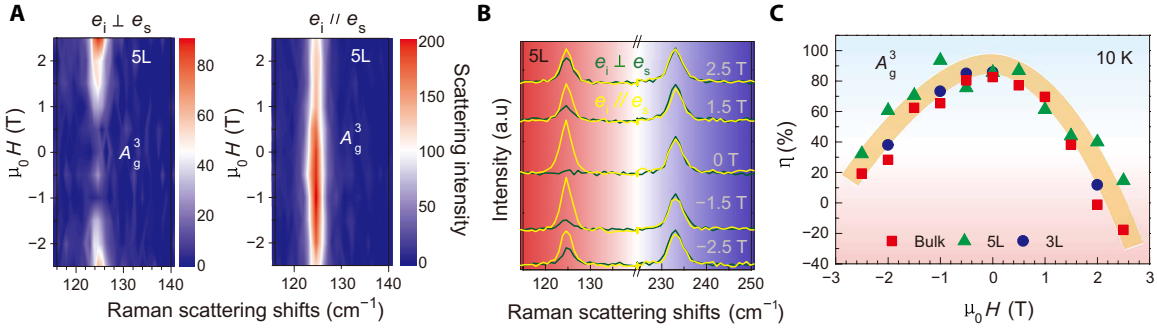


**Fig. 4. Experimental results on magnetic control of degree of polarization.** (**A** and **B**) Raman scattering spectra of 5L $CrI_3$ in the perpendicular and parallel polarization configurations as a function of magnetic field. The $A_g^3$ mode intensity can be controlled by a magnetic field and display an opposite magnetic field dependence in perpendicular and parallel configurations. (**C**) Degree of polarization as a function of magnetic field.

Figure 4 (A and B) shows the magnetophonon Raman scattering intensity in the two-polarization configurations as a function of magnetic field. The Raman scattering intensity in the cross-polarization configuration increases as the magnetic field increases, whereas the Raman intensity in the parallel-polarization configuration decreases. The DOP, defined as $\eta = (I_{//} - I_{\perp})/(I_{//} + I_{\perp})$, is up to ~85% and can be tuned monotonically from −20 to 85% when the magnetic field decreases from ±2.5 T to 0 (Fig. 4C). These results raise the feasibility of applying 2D ferromagnetic few-layer $CrI_3$ for information encoding and data storage.

## CONCLUSION

In summary, a giant nonreciprocal magnetophonon effect is observed in ferromagnetic few-layer $CrI_3$. The magnetic control of anisotropic Raman scattering, in which the polarization angle, ellipticity, and DOP are magnetic field dependent, has been demonstrated. The nonreciprocal magnetophonon scattering originates from magnetically controlling the natural frequency by Lorentz force, leading to the nonreciprocally magnetic manipulation of diagonal components and off-diagonal components of the polarizability tensor. Our results demonstrate the unique potential of 2D ferromagnets for magnetically controlled information encoding and Raman lasing applications.

## MATERIALS AND METHODS

### $CrI_3$ synthesis and preparation

The $CrI_3$ bulk crystals were synthesized by the chemical vapor transport method. Chromium powder (99.99%, Alfa Aesar) and anhydrous iodine particles (99.99%, Alfa Aesar) were mixed stoichiometrically. About 1 g of the mixture was loaded in the ampoule (16-mm inner diameter, 20-mm outer diameter, and 200-mm length). The ampoule with the mixture was placed into liquid nitrogen to prevent sublimation of iodine particles and then evacuated to a pressure of approximately $10^{-3}$ Pa. The ampoule was sealed and placed into a two-zone furnace with temperature gradient of 650° to 530°C for 7 days. The $CrI_3$ crystal that is shiny and black was obtained at the sink region of the ampoule. The crystal was stored in a nitrogen atmosphere and in anhydrous conditions.

The few-layer $CrI_3$ flakes were mechanically exfoliated from bulk crystal onto polydimethylsiloxane films and then directly transferred onto $SiO_2$/Si substrates, which were in situ–loaded into the cold head for optical measurements in the glove box.

### Raman measurements

The Raman signals were recorded by a Witec Alpha 300R Plus confocal Raman microscope, which is coupled with a closed-cycle He optical cryostat (10 K) and a superconducting magnet. A long work distance 50× objective (numerical aperture = 0.45) was used for the Raman measurement at 10 K and magnetic field. The Raman signals were first collected by a photonic crystal fiber and then coupled into the spectrometer with 1800 g/mm grating. The polarization-resolved Raman spectra were obtained by rotating the polarization of the analyzer, which was put before the photonic crystal fiber. The power of the excitation laser at 514 nm was measured to about 2 mW, and the typical integration time is 20 s. The magneto-optical system is checked by angle-resolved polarized Raman spectra using highly ordered pyrolytic graphite (HOPG) as reference samples; the G mode intensities of HOPG are isotropic on its basal plane, verifying that our optical system is excellently calibrated (see section S2).

## SUPPLEMENTARY MATERIALS

Supplementary material for this article is available at http://advances.sciencemag.org/cgi/content/full/6/43/eabc7628/DC1

## REFERENCES AND NOTES

1. N. D. Mermin, H. Wagner, Absence of ferromagnetism or antiferromagnetism in one- or two-dimensional isotropic Heisenberg models. *Phys. Rev. Lett.* **17**, 1133–1136 (1966).
2. C. Gong, L. Li, Z. Li, H. Ji, A. Stern, Y. Xia, T. Cao, W. Bao, C. Wang, Y. Wang, Z. Q. Qiu, R. J. Cava, S. G. Louie, J. Xia, X. Zhang, Discovery of intrinsic ferromagnetism in two-dimensional van der Waals crystals. *Nature* **546**, 265–269 (2017).
3. B. Huang, G. Clark, E. Navarro-Moratalla, D. R. Klein, R. Cheng, K. L. Seyler, D. Zhong, E. Schmidgall, M. A. McGuire, D. H. Cobden, W. Yao, D. Xiao, P. Jarillo-Herrero, X. Xu, Layer-dependent ferromagnetism in a van der Waals crystal down to the monolayer limit. *Nature* **546**, 270–273 (2017).
4. Y. Zhang, X. Wu, B. Lyu, M. Wu, S. Zhao, J. Chen, M. Jia, C. Zhang, L. Wang, X. Wang, Y. Chen, J. Mei, T. Taniguchi, K. Watanabe, H. Yan, Q. Liu, L. Huang, Y. Zhao, M. Huang, Magnetic order-induced polarization anomaly of raman scattering in 2D magnet $CrI_3$. *Nano Lett.* **20**, 729–734 (2020).
5. Y. Deng, Y. Yu, Y. Song, J. Zhang, N. Z. Wang, Z. Sun, Y. Yi, Y. Z. Wu, S. Wu, J. Zhu, J. Wang, X. H. Chen, Y. Zhang, Gate-tunable room-temperature ferromagnetism in two-dimensional $Fe_3GeTe_2$. *Nature* **563**, 94–99 (2018).
6. N. Mounet, M. Gibertini, P. Schwaller, D. Campi, A. Merkys, A. Marrazzo, T. Sohier, I. E. Castelli, A. Cepellotti, G. Pizzi, N. Marzari, Two-dimensional materials from

high-throughput computational exfoliation of experimentally known compounds. *Nat. Nanotechnol.* **13**, 246–252 (2018).
7. M. Bonilla, S. Kolekar, Y. Ma, H. C. Diaz, V. Kalappattil, R. Das, T. Eggers, H. R. Gutierrez, M.-H. Phan, M. Batzill, Strong room-temperature ferromagnetism in $VSe_2$ monolayers on van der Waals substrates. *Nat. Nanotechnol.* **13**, 289–293 (2018).
8. J.-U. Lee, S. Lee, J. H. Ryoo, S. Kang, T. Y. Kim, P. Kim, C.-H. Park, J.-G. Park, H. Cheong, Ising-type magnetic ordering in atomically thin $FePS_3$. *Nano Lett.* **16**, 7433–7438 (2016).
9. D. L. Sounas, A. Alù, Non-reciprocal photonics based on time modulation. *Nat. Photonics* **11**, 774–783 (2017).
10. A. K. Zvezdin, V. A. Kotov, Eds., *Modern Magnetooptics and Magnetooptical Materials* (Taylor & Francis Group, 1997).
11. M. Inoue, M. Levy, A. V. Baryshev, *Magnetophotonics: From Theory to Applications* (Springer, 2013).
12. D. R. Klein, D. MacNeill, J. L. Lado, D. Soriano, E. Navarro-Moratalla, K. Watanabe, T. Taniguchi, S. Manni, P. Canfield, J. Fernández-Rossier, P. Jarillo-Herrero, Probing magnetism in 2D van der Waals crystalline insulators via electron tunneling. *Science* **360**, 1218–1222 (2018).
13. T. Song, X. Cai, M. W.-Y. Tu, X. Zhang, B. Huang, N. P. Wilson, K. L. Seyler, L. Zhu, T. Taniguchi, K. Watanabe, M. A. McGuire, D. H. Cobden, D. Xiao, W. Yao, X. Xu, Giant tunneling magnetoresistance in spin-filter van der Waals heterostructures. *Science* **360**, 1214–1218 (2018).
14. Z. Sun, Y. Yi, T. Song, G. Clark, B. Huang, Y. Shan, S. Wu, D. Huang, C. Gao, Z. Chen, M. McGuire, T. Cao, D. Xiao, W.-T. Liu, W. Yao, X. Xu, S. Wu, Giant nonreciprocal second-harmonic generation from antiferromagnetic bilayer $CrI_3$. *Nature* **572**, 497–501 (2019).
15. K. L. Seyler, D. Zhong, D. R. Klein, S. Gao, X. Zhang, B. Huang, E. Navarro-Moratalla, L. Yang, D. H. Cobden, M. A. McGuire, W. Yao, D. Xiao, P. Jarillo-Herrero, X. Xu, Ligand-field helical luminescence in a 2D ferromagnetic insulator. *Nat. Phys.* **14**, 277–281 (2017).
16. Z. Wang, I. Gutiérrez-Lezama, N. Ubrig, M. Kroner, M. Gibertini, T. Taniguchi, K. Watanabe, A. Imamoğlu, E. Giannini, A. F. Morpurgo, Very large tunneling magnetoresistance in layered magnetic semiconductor $CrI_3$. *Nat. Commun.* **9**, 2516 (2018).
17. M. A. McGuire, H. Dixit, V. R. Cooper, B. C. Sales, Coupling of crystal structure and magnetism in the layered, ferromagnetic insulator $CrI_3$. *Chem. Mater.* **27**, 612–620 (2015).
18. M. Arai, R. Moriya, N. Yabuki, S. Masubuchi, K. Ueno, T. Machida, Construction of van der Waals magnetic tunnel junction using ferromagnetic layered dichalcogenide. *Appl. Phys. Lett.* **107**, 103107 (2015).
19. S. Jiang, J. Shan, K. F. Mak, Electric-field switching of two-dimensional van der Waals magnets. *Nat. Mater.* **17**, 406–410 (2018).
20. S. Jiang, L. Li, Z. Wang, K. F. Mak, J. Shan, Controlling magnetism in 2D $CrI_3$ by electrostatic doping. *Nat. Nanotechnol.* **13**, 549–553 (2018).
21. B. Huang, G. Clark, D. R. Klein, D. MacNeill, E. Navarro-Moratalla, K. L. Seyler, N. Wilson, M. A. McGuire, D. H. Cobden, D. Xiao, W. Yao, P. Jarillo-Herrero, X. Xu, Electrical control of 2D magnetism in bilayer $CrI_3$. *Nat. Nanotechnol.* **13**, 544–548 (2018).
22. T. Li, S. Jiang, N. Sivadas, Z. Wang, Y. Xu, D. Weber, J. E. Goldberger, K. Watanabe, T. Taniguchi, C. J. Fennie, K. Fai Mak, J. Shan, Pressure-controlled interlayer magnetism in atomically thin $CrI_3$. *Nat. Mater.* **18**, 1303–1308 (2019).
23. T. Song, Z. Fei, M. Yankowitz, Z. Lin, Q. Jiang, K. Hwangbo, Q. Zhang, B. Sun, T. Taniguchi, K. Watanabe, M. A. McGuire, D. Graf, T. Cao, J.-H. Chu, D. H. Cobden, C. R. Dean, D. Xiao, X. Xu, Switching 2D magnetic states via pressure tuning of layer stacking. *Nat. Mater.* **18**, 1298–1302 (2019).
24. B. Huang, J. Cenker, X. Zhang, E. L. Ray, T. Song, T. Taniguchi, K. Watanabe, M. A. McGuire, D. Xiao, X. Xu, Tuning inelastic light scattering via symmetry control in the two-dimensional magnet $CrI_3$. *Nat. Nanotechnol.* **15**, 212–216 (2020).
25. C. Faugeras, M. Amado, P. Kossacki, M. Orlita, M. Sprinkle, C. Berger, W. A. de Heer, M. Potemski, Tuning the electron-phonon coupling in multilayer graphene with magnetic fields. *Phys. Rev. Lett.* **103**, 186803 (2009).
26. M. Kühne, C. Faugeras, P. Kossacki, A. A. L. Nicolet, M. Orlita, Y. I. Latyshev, M. Potemski, Polarization-resolved magneto-Raman scattering of graphenelike domains on natural graphite. *Phys. Rev. B* **85**, 195406 (2012).
27. B. Zhao, Y. Shi, J. Wang, Z. Zhao, N. Zhao, S. Fan, Near-complete violation of Kirchhoff's law of thermal radiation with a 0.3 T magnetic field. *Opt. Lett.* **44**, 4203–4206 (2019).
28. J. Ji, A. Zhang, J. Fan, Y. Li, X. Wang, J. Zhang, E. W. Plummer, Q. Zhang, Giant magneto-optical Raman effect in a layered transition metal compound. *Proc. Natl. Acad. Sci. U.S.A.* **113**, 2349–2353 (2016).
29. H. Rong, A. Liu, R. Jones, O. Cohen, D. Hak, R. Nicolaescu, A. Fang, M. Paniccia, An all-silicon Raman laser. *Nature* **433**, 292–294 (2005).
30. H. Rong, R. Jones, A. Liu, O. Cohen, D. Hak, A. Fang, M. Paniccia, A continuous-wave Raman silicon laser. *Nature* **433**, 725–728 (2005).
31. M. Yu, Y. Okawachi, R. Cheng, C. Wang, M. Zhang, A. L. Gaeta, M. Lončar, Raman lasing and soliton mode-locking in lithium niobate microresonators. *Light Sci. Appl.* **9**, 9 (2020).
32. O. Boyraz, B. Jalali, Demonstration of a silicon Raman laser. *Opt. Express* **12**, 5269–5273 (2004).
33. K. Guo, B. Deng, Z. Liu, C. Gao, Z. Shi, L. Bi, L. Zhang, H. Lu, P. Zhou, L. Zhang, Y. Cheng, B. Peng, Layer dependence of stacking order in nonencapsulated few-layer $CrI_3$. *Sci. China Mater.* **63**, 413–420 (2020).
34. S. Djurdjić-Mijin, A. Šolajić, J. Pešić, M. Šćepanović, Y. Liu, A. Baum, C. Petrovic, N. Lazarević, Z. V. Popović, Lattice dynamics and phase transition in $CrI_3$ single crystals. *Phys. Rev. B* **98**, 104307 (2018).
35. D. Shcherbakov, P. Stepanov, D. Weber, Y. Wang, J. Hu, Y. Zhu, K. Watanabe, T. Taniguchi, Z. Mao, W. Windl, J. Goldberger, M. Bockrath, C. N. Lau, Raman spectroscopy, photocatalytic degradation, and stabilization of atomically thin chromium tri-iodide. *Nano Lett.* **18**, 4214–4219 (2018).
36. L. Webster, L. Liang, J.-A. Yan, Distinct spin-lattice and spin-phonon interactions in monolayer magnetic $CrI_3$. *Phys. Chem. Chem. Phys.* **20**, 23546–23555 (2018).
37. W. Zhao, Q. Wu, Q. Hao, J. Wang, M. Li, Y. Zhang, K. Bi, Y. Chen, Z. Ni, Plasmon-phonon coupling in monolayer $WS_2$. *Appl. Phys. Lett.* **108**, 131903 (2016).
38. J. F. Dillon Jr., H. Kamimura, J. P. Remeika, Magneto-optical properties of ferromagnetic chromium trihalides. *J. Phys. Chem. Solids* **27**, 1531–1549 (1966).
39. J. Suits, Faraday and Kerr effects in magnetic compounds. *IEEE Trans. Magn.* **8**, 95–105 (1972).
40. Z. Q. Qiu, S. D. Bader, Surface magneto-optic Kerr effect. *Rev. Sci. Instrum.* **71**, 1243–1255 (2000).
41. M. C. Onbasli, L. Beran, M. Zahradník, M. Kučera, R. Antoš, J. Mistrík, G. F. Dionne, M. Veis, C. A. Ross, Optical and magneto-optical behavior of Cerium Yttrium Iron Garnet thin films at wavelengths of 200–1770 nm. *Sci. Rep.* **6**, 23640 (2016).
42. W. Fu, X. Zhao, K. Wang, Z. Chen, K. Leng, D. Fu, P. Song, H. Wang, L. Deng, S. J. Pennycook, G. Zhang, B. Peng, K. P. Loh, An anomalous magneto-optic effect in epitaxial indium selenide layers. *Nano Lett.* **20**, 5330–5338 (2020).

**Acknowledgments**

**Funding:** We acknowledge the financial support from the National Science Foundation of China (51602040, 51872039, and 51972046) and the Science and Technology Program of Sichuan (M112018JY0025). C.-W.Q. acknowledges financial support from A*STAR Pharos Program (grant number 15270 00014, with project number R-263-000-B91-305) and the National Research Foundation, Prime Minister's Office, Singapore under Competitive Research Program Award NRF-CRP22-2019-0006. **Author contributions:** B.P., L.D., and C.-W.Q. developed the concept, designed the experiment, and prepared the manuscript. Y.C. and S.L. synthesized the $CrI_3$ crystal. K.G., Z.L., Z.S., and Y.L. prepared the $CrI_3$ samples, performed the polarization-resolved Raman measurements, and studied temperature dependence. P.-H.T., L.B., G.H., C.-W.Q., M.-L.L., X.L.L., Linbo Zhang, H.C., Li Zhang, H.L., P.Z., and J.X. contributed to the discussion of the mechanism of magneto-optical scattering effect. All authors contributed to the editing and revision of the manuscript. **Competing interests:** The authors declare that they have no competing interests. **Data and materials availability:** All data needed to evaluate the conclusions in the paper are present in the paper and/or the Supplementary Materials. Additional data related to this paper may be requested from the authors.

Submitted 12 May 2020
Accepted 3 September 2020
Published 23 October 2020
10.1126/sciadv.abc7628

**Citation:** Z. Liu, K. Guo, G. Hu, Z. Shi, Y. Li, L. Zhang, H. Chen, L. Zhang, P. Zhou, H. Lu, M.-L. Lin, S. Liu, Y. Cheng, X. L. Liu, J. Xie, L. Bi, P.-H. Tan, L. Deng, C.-W. Qiu, B. Peng, Observation of nonreciprocal magnetophonon effect in nonencapsulated few-layered $CrI_3$. *Sci. Adv.* **6**, eabc7628 (2020).

Science Advances

# Observation of nonreciprocal magnetophonon effect in nonencapsulated few-layered $CrI_3$

Zhen Liu, Kai Guo, Guangwei Hu, Zhongtai Shi, Yue Li, Linbo Zhang, Haiyan Chen, Li Zhang, Peiheng Zhou, Haipeng Lu, Miao-Ling Lin, Sizhao Liu, Yingchun Cheng, Xue Lu Liu, Jianliang Xie, Lei Bi, Ping-Heng Tan, Longjiang Deng, Cheng-Wei Qiu and Bo Peng

*Sci Adv* **6** (43), eabc7628.
DOI: 10.1126/sciadv.abc7628